Design and Optimization of a Voice Coil Motor With a Rotary Actuator for an Ultrasound Scanner

Kristopher J. Smith, David J. Graham, and Jeffrey A. Neasham

***Abstract*—This paper proposes a new application for the rotary voice coil motor (VCM). In developing a low-cost ultrasound scanner for the developing world, an oscillating transducer is required to sweep over the skin. The ultrasound scanner must operate from a USB power supply in remote locations. The application requires a 3.3-N force on the coils of the motor to overcome the inertia of the skin. A proof-of-concept prototype motor with electronics has been designed, simulated, and tested. The VCM optimization is discussed in detail with the unique separation of the magnets being critical to reduce the axial bearing forces for this application.**

***Index Terms*—Permanent-magnet (PM) motor, rotary actuator, 3-D finite-element analysis (FEA), voice coil motor (VCM).**

I. Introduction

ULTRASOUND imaging is commonly used as a noninvasive diagnostic tool, which employs either a linear, curved, or 2-D array of transducer elements [1]–[3]. Generally, it is considered that the image quality and cost are proportional to the number of transducer elements [4]. As the number of elements increases, so does the associated electronics, which are required to transmit and receive on each element. The construction of multichannel phase array transducer would far exceed the target cost of this project. Thus, a single transducer element design will be used, which will require an actuator to create a synthetic array by mechanically moving the transducer. This method of combining a single transducer element and a mechanical actuator is unique in the context of modern medical ultrasound imaging [5]–[8]. This is a compromise as the image quality is reduced but the cost saving is significant (over 95% cost reduction). Fig. 1 shows a typical commercially available ultrasound probe compared with the prototype single-element transducer.

The process for controlling the ultrasound scanner is shown in Fig. 2. The single transducer element is periodically activated at 0.25° increments over the scanning arm cycle. At each increment, a short pulse of 4.2-MHz ultrasound is transmitted, and the echo data are received, synthetically replicating a 200-element transducer array.

Fig. 1. Comparison of the (left) SonoSite multichannel array transducer [9] and the (right) prototype single-element ultrasound scanner.

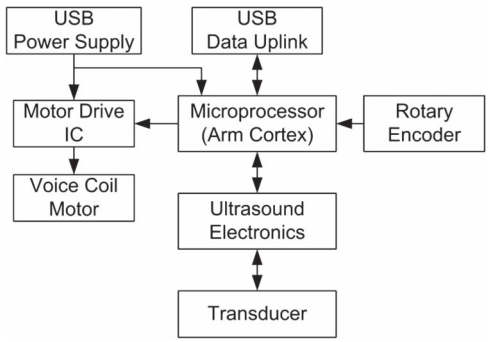

Fig. 2. Ultrasound scanner hardware control process.

The low electrical noise of the permanent-magnet (PM) rotary actuator voice coil motor (VCM) is ideal for maintaining a high signal-to-noise ratio of the echo data, and the accurate positional encoder allows the ultrasound image to be constructed at the end of each scanning cycle.

The VCM rotary actuator shown in Fig. 3 is commonly utilized in hard disk drives (HDDs) and optical storage devices, i.e., the Blu-ray disk [10], [11]. The VCM is continually improved to reduce vibration [12], cope with the increase in volumetric density [13], and develop the control design for head positioning [14]. In recent years, it has been used for lens focusing and zooming on mobile camera phones due to the low current demands [15], [16]. The VCM is also applied to linear actuators, which have wide applications in transportation and manufacturing [17], [18]. This paper describes a new application where the VCM is used to drive the swing arm of a portable low-cost ultrasound scanner. The typical VCM

Manuscript received December 8, 2014; revised April 28, 2015; accepted May 15, 2015. Date of publication June 24, 2015; date of current version October 7, 2015. This work was supported in part by the Engineering and Physical Sciences Research Council, via the Impact Acceleration Account, and in part by Delft Imaging Systems.

The authors are with the School of Electrical and Electronic Engineering, Newcastle University, Newcastle upon Tyne, NE1 7RU, U.K. (e-mail: kristopher.smith@ncl.ac.uk).

Color versions of one or more of the figures in this paper are available online at http://ieeexplore.ieee.org.

Digital Object Identifier 10.1109/TIE.2015.2449780

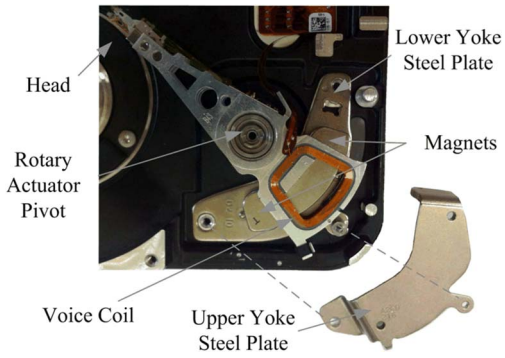

Fig. 3. Configuration of a computer HDD with VCM.

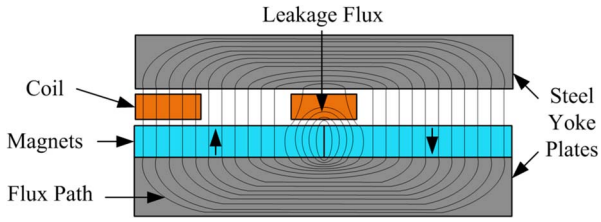

Fig. 4. Two-dimensional conventional single-sided VCM.

of an HDD or an optical storage device has a peak force of around 0.1 N to sweep the head over the storage disk [10], [19]. The design challenge of the ultrasound scanner requires a force profile, which is 33 times larger in magnitude compared with the standard VCM design. The ultrasound scanner will have a strict USB 5-V 500-mA power supply with the VCM current limited to 300 mA, given that 200 mA is required for electronic control and periodic ultrasound data acquisition.

The VCM rotary actuator is directly coupled to the load, with no gears, cogs, or brushes. This increases the motor life expectancy due to the limited number of moving parts and offers high reliability [10], [20]. The VCM-controlled swing arm will operate at 2 Hz, which will have low acoustic noise (compared with a geared system), but, more importantly, low electrical noise and simple control. The use of PM materials ensures a high torque-density-to-current ratio [21], [22]. However, rare-earth materials have the problem of high cost and limited supply [23].

The most common topology of the VCM for optical disk drives is shown in Fig. 4 [24], [25]. The magnets are located on a single side, where the magnet placement creates flux leakage in the air gap, which can cause an unwanted axial force.

In Fig. 5, an adaption of the Halbach [26], [27] magnetic circuit for the rotary VCMs was introduced by Sung *et al.* [28]. The Halbach approach was applied by Choi *et al.* [29] to an HDD. It found, for the same magnetic circuit volume (compared with a conventional VCM), that the dynamic force increased by 11%, but utilized 33% more magnet (due to the reduction in yoke flux saturation), thus improving the air-gap flux density for a limited magnetic circuit volume. It also showed that, when using the same magnet mass for both conventional and Halbach designs, it offers little performance difference [29]. However, the Halbach will have an increased manufacturing complexity and associated cost.

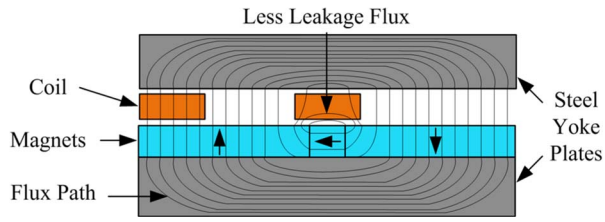

Fig. 5. Two-dimensional Halbach-approach single-sided VCM.

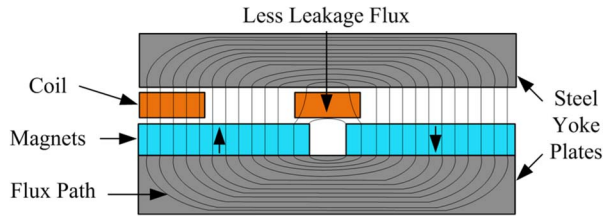

Fig. 6. Two-dimensional separated-magnet single-sided VCM.

The VCM operation is based on the Lorentz force principle, where, by driving a current through the voice coil placed in a PM field, a force will act upon the voice coil. If the voice coil is perpendicular to the PM field, it can be seen that

$$F = I\beta LN \tag{1}$$

where the resultant force F on the coil is proportional to the current I, magnetic flux density β, coil length L, and the number of turns N within the PM field. In the conventional and Halbach VCM designs, as the current-carrying wire is moved above the magnet intersection, the force imposed by the leakage flux produces an unwanted axial force on the bearings, pushing the coil toward the steel yoke. Thus, part of the magnet and magnetic field is wasted. This axial force has the potential to distort the path taken by the transducer as it sweeps. Any axial deflection will result in image distortion because it is assumed that each data acquisition point lies perfectly on a 2-D arc. Fig. 6 shows the new topology VCM to reduce this axial force, where the magnets are separated to achieve less leakage flux.

II. Design of VCM Rotary Actuator

The application of using the VCM within the swing arm of an ultrasound scanner requires a sufficient force to overcome the inertia of the scanning head moving across the skin in a layer of coupling gel. From experimental results, by attaching the ultrasound scanning head to a Sauter Digital Force Gauge FK50, it was ascertained that a peak 1.5-N force is required at the scanning arm tip. The design of the casing limits the VCM position to be half the distance from the actuator pivot point to that of the scanning head. Thus, the VCM will need to generate a peak 3.3-N force acting on the coils (this includes a 10% margin of safety into the force requirement).

Fig. 7 shows the ultrasound casing, which is designed to limit the actuator swing arm to a range of 50°. The voice coil size is limited to fit inside the coil support mount ensuring a maximum size of L50 × W30 mm.

The USB-operated ultrasound limits the power available for the VCM to 1.5 W (5 V at 300 mA) to allow normal device

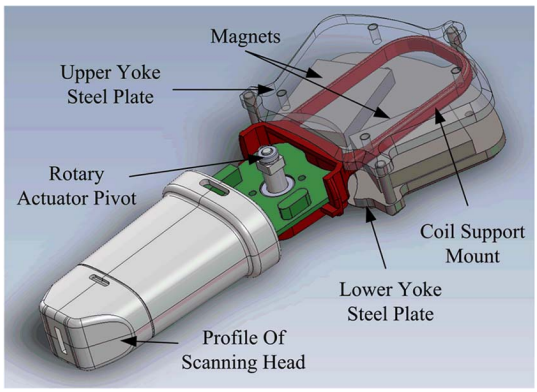

Fig. 7. Ultrasound scanner computer-aided design (CAD) housing.

TABLE I
VOICE COIL DESIGN

Model	Turns	Coil Area (mm^2)	Standard Wire OD (mm)	Coil Resistance (Ω)	Lorentz Force (N)
1	200	10	0.18	16.4	1.8
2	300	23	0.224	16.0	2.7
3	320	25.2	0.224	16.6	2.9
4	340	26.9	0.224	17.6	3.1
5	340	33.3	0.25	14.2	3.1
6	360	35.3	0.25	15.1	3.2
7	380	37.2	0.25	15.9	3.4
8	400	40	0.25	16.4	3.6

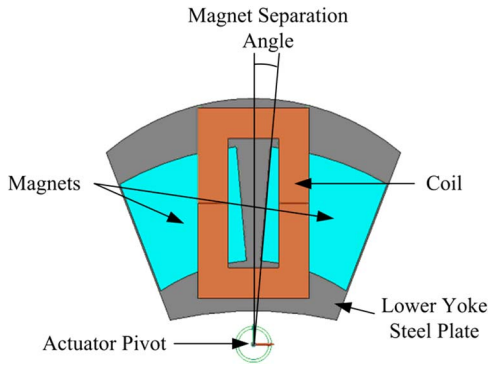

Fig. 8. VCM top view (upper yoke removed).

operation. Thus, the voice coil resistance is ideally designed at 16.6 Ω to achieve simple current limiting. Using the Lorentz principle (1), the following voice coil forces can be calculated in Table I.

Thus, the VCM design that satisfies the 3.3-N peak force requirement is Model 7 (see Table I), which has 380 turns, requiring a coil area of 37.2 mm^2, assuming a 50% fill factor.

III. FE SIMULATION AND ANALYSIS

The Infolytica MagNet (version 7.4) 3-D finite-element (FE) simulation package is used to determine the magnetic field distribution for the VCM. Figs. 8 and 9 show the proposed structure of the actuator.

To design the optimal VCM for this application, the coil parameters have been calculated using the Lorentz force (see

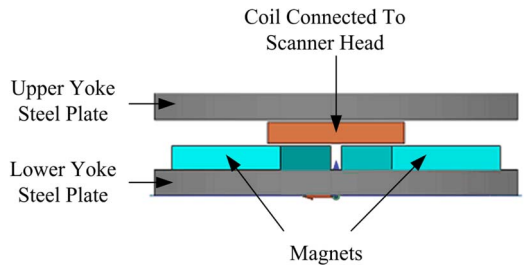

Fig. 9. VCM side view.

TABLE II
VCM PARAMETER RANGE

Symbol	Machine Parameters	Value	Units
MH	Magnet Height	1,2,3,4,5,6,7,8,9,10	mm
MS	Angle of Magnet Separation	0,2.5,5,7.5,10,12.5,15	degrees
IRE	Magnet Inner Radius Extension	0,1,2,3,4,5,6,7,8,9,10	mm
ORE	Magnet Outer Radius Extension	01,2,3,4,5,6,7,8,9,10	mm
cl	Coil Length	50	mm
c	Coil Inner Length	34	mm
cw	Coil Width	30	mm
ct	Coil Winding Thickness	8	mm
ml	Magnet Length	30	mm
	Lower Yoke Height	8	mm
	Upper Yoke Height	8	mm
	Air Gap	0.5	mm

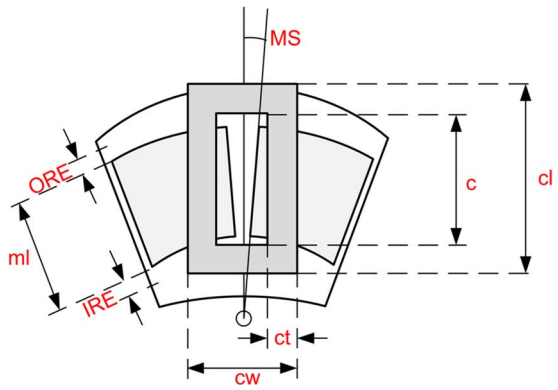

Fig. 10. VCM parameters and structure.

Table I) and designed based on the geometric case limits. The magnet size and position are optimized through the 3-D FE parametric variation analysis. The yoke steel plates completing the electromagnet circuit are restricted to 8 mm thick to avoid high flux saturation and reduced torque capability during the optimization process [30], [31], although, practically, they need to be as thin as possible for practical device weight savings. A summary of the optimization parameters is shown in Table II.

Fig. 10 identifies the motor design parameters outlined in Table II.

IV. OPTIMIZATION PROCESS AND ANALYSIS

Through a variable matrix controller, the design parameters are changed. The optimization will be assessed by an objective function to identify the best design. The objective function is the maximization of the scanning arm force with the minimization of bearing axial force while using the smallest amount of

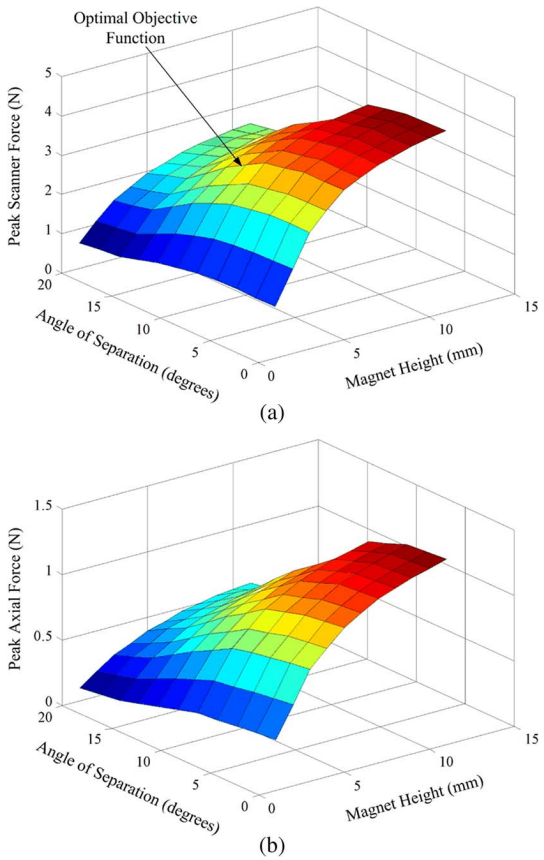

Fig. 11. Three-dimensional FEA parameter optimization results for MS and MH. (a) Peak scanning force. (b) Peak axial force.

magnet to satisfy the 3.3-N scanner requirement. This can be represented as

$$f_{\text{OBJECTIVE}} = \max \times \left\{ \frac{\text{Force}_{\text{PEAK SCANNER}} - \text{Force}_{\text{PEAK AXIAL}}}{\text{Magnet Mass}} \right\} \quad (2)$$

with

$$\text{Force}_{\text{PEAK SCANNER}} >= 3.3.$$

As the magnet height (MH) increases and the angle of magnet separation (MS) decreases, the total magnet mass used is increased, thus increasing the air-gap flux density, which, in turn, causes the peak force applied to the scanning head and the axial force applied to the bearing to increase.

Analyzing Fig. 11, the objective function identifies the optimal design with a magnet height of 5 mm and a 10° magnet separation angle, which uses 55 g of neodymium magnet. The graphical trend also confirms that, during the optimization process, as the angle of magnet separation (MS) increases, the axial force imposed on the bearings decreases due to the leakage flux reduction. This is highlighted in Fig. 12, which shows the flux path for a conventional and separated-magnet VCMs with the same magnet mass. The flux leakage above the magnet intersection is 0.7 and 0.1 T, respectively. Thus, changing the design to separate the magnets reduces the axial

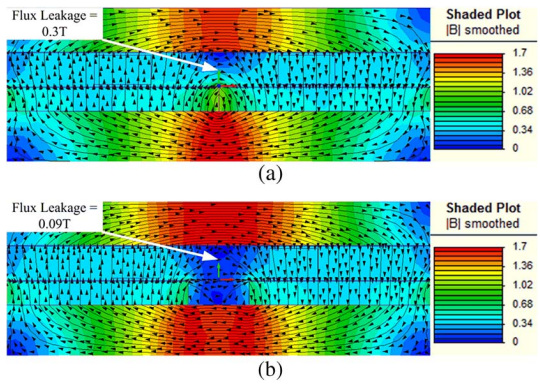

Fig. 12. Two-dimensional flux paths of (a) conventional VCM and (b) separated-magnet VCM.

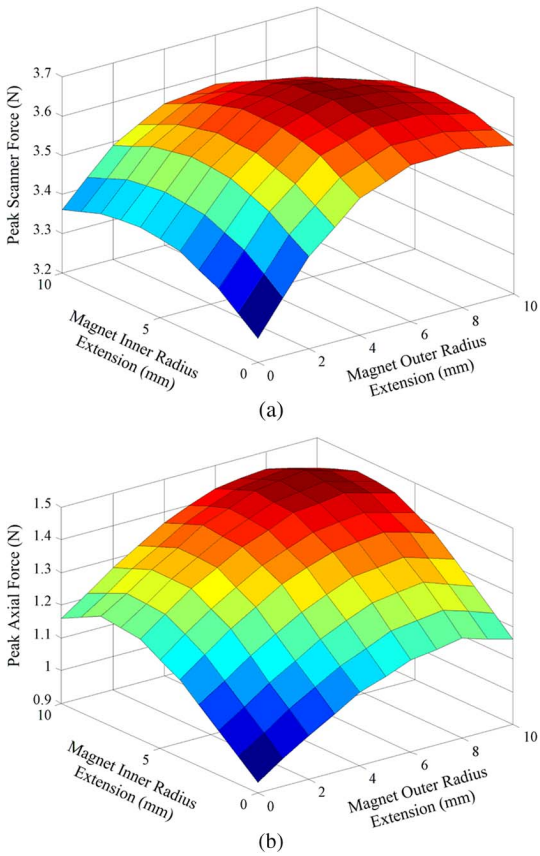

Fig. 13. Three-dimensional FEA parameter optimization results for IRE and ORE. (a) Peak scanning force. (b) Peak axial force.

force on the bearing to allow a smooth scanning motion, while increasing the bearings life expectancy.

The placement of the magnet relative to the coil design has a significant effect on the rotary arm and axial forces. Fig. 10 has shown the magnet inner and outer radius edges fall 2 mm (c-ml) away from the coil inner edges during the MS and MH optimization. As the magnet edges outer radius (ORE) and inner radius (IRE) are extended, they will fall directly under the top and bottom sections of the coil. The resultant effect of the magnet extension is shown in Fig. 13. The results identify that, as the ORE and the IRE are extended, the best case scanning

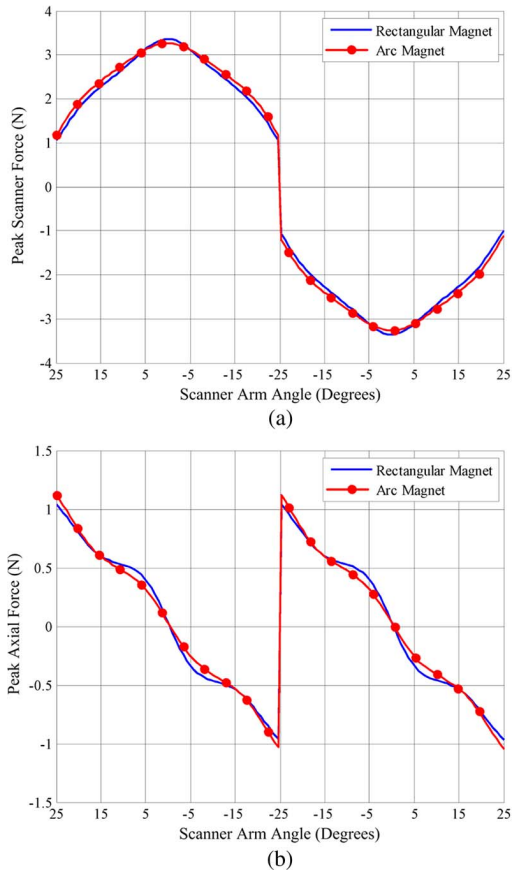

Fig. 14. Three-dimensional FEA comparison of arc and rectangular magnets. (a) Scanning force. (b) Axial force.

head force increases by 11%, whereas the worst case axial bearing force increases by 43%.

V. Simulated Final Optimized Design for Practical Implementation

For fabrication, a rectangular magnet is used to replace the arc magnet discussed in the optimization process. This allows off-the-shelf magnets to be purchased, reducing prototyping time and costs. Thus, the experimental results in Section VI are compared with an updated FE model. Fig. 14 shows a comparison of the arc magnet and the rectangular magnet (L30 × W25 × H5 mm) over a complete mechanical scanner cycle. The peak and mean forces change by less than 3% for the scanning and axial forces. Thus, the rectangular magnet is considered a suitable replacement to achieve the required motor performance.

VI. Fabrication and Experimental Results

After the VCM optimization, a prototype machine, as shown in Fig. 15, is built for experimental validation. The motor is driven by a 5-V USB power supply. The force measurements are taken using the Sauter Digital Force Gauge FK50.

The results for the simulated and experimental machine testing are shown in Fig. 16. The axial forces could not be measured as the force is reduced so that the pivot bearings limit any axial motion. The experimental results for the scanning force are

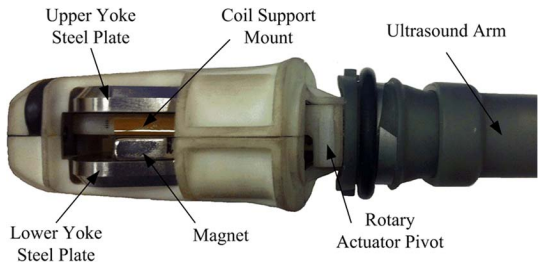

Fig. 15. Prototype VCM machine design for the ultrasound scanner.

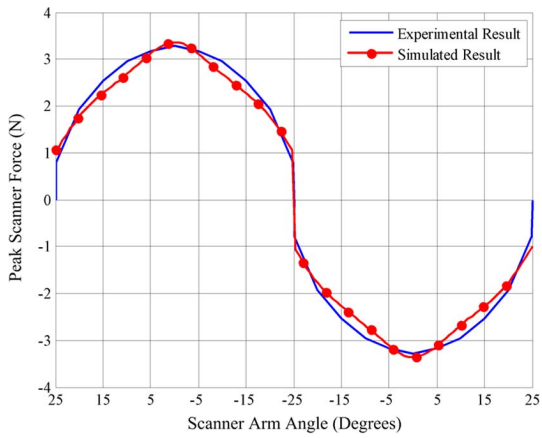

Fig. 16. Comparing VCM experimental and 3-D FEA simulation results of the scanning force.

within 10% of the estimated 3-D FE analysis (FEA) simulation. Using a Gauss meter probe, the experimental machine yields a 10% higher air-gap flux density than that of the simulated model. Thus, taking into account manufacturing tolerance of magnets, air gaps, and the housing construction, this shows a good correlation between the experimental and simulation results.

VII. Conclusion

A new magnet topology VCM rotary actuator has been designed and experimentally verified for the ultrasound scanner application. The experimental results are in good agreement with the predicted 3-D FEA simulation, confirming the suitability of the motor for this application.

The VCM optimization covers the unique magnet placement and angle of separation required to reduce the axial bearing forces. The simulation results show that, by separating the magnets, the air-gap leaking flux density has dropped by 85% from 0.7 to 0.1 T. This reduces the axial force and limits any deviation from the desired transducer movement arc, which would result in image distortion.

The cost of the VCM motor components and drive electronics for the prototype machine is approximately $11, with the magnets accounting for nearly 70% of the total cost. Future work involves analyzing a double-sided VCM for a flatter force profile and simultaneously changing the magnet material to ferrite to see if the same performance can be achieved at an even cheaper cost.

REFERENCES

[1] G. Matrone, F. Quaglia, and G. Magenes, "Modeling and simulation of ultrasound fields generated by 2D phased array transducers for medical applications," in *Proc. Annu. Int. Conf. IEEE EMBC*, 2010, pp. 6003–6006.

[2] A. Fenster, G. Parraga, and J. Bax, "Three-dimensional ultrasound scanning," *Interface Focus*, vol. 1, no. 4, pp. 503–519, Aug. 2011.

[3] R. W. Prager, U. Z. Ijaz, A. H. Gee, and G. M. Treece, "Three-dimensional ultrasound imaging," *Proc. Inst. Mech. Eng., J. Eng. Med.*, vol. 224, no. 2, pp. 193–223, Feb. 2010.

[4] F. Aaron, B. D. Dónal, and H. N. Cardinal, "Three-dimensional ultrasound imaging," *Phys. Med. Biol.*, vol. 46, no. 5, pp. R67–R99, May 2001.

[5] J. Neasham and D. Graham, "Ultrasound imaging apparatus," U.K. Patent GB 2515601, Dec. 31, 2014.

[6] J. Neasham and D. Graham, "Ultrasound imaging apparatus," U.S. Patent 13 974 483, Sep. 18, 2014.

[7] J. Neasham and D. Graham, "Ultrasound imaging apparatus," WO 2014140557 A1, Sep. 18, 2014.

[8] A. Gee, R. Prager, G. Treece, and L. Berman, "Engineering a freehand 3D ultrasound system," *Pattern Recognit. Lett.*, vol. 24, no. 4/5, pp. 757–777, Feb. 2003.

[9] SonoSite Ultrasound Transducer C60N. [Online]. Available: http://www.sonosite.com/

[10] D.-J. Lee *et al.*, "Design of swing arm actuator for small and slim optical disc drives," *Microsyst. Technol.*, vol. 13, no. 8–10, pp. 1307–1313, May 2007.

[11] E. J. Hong *et al.*, "Design of swing arm type actuator and suspension for micro optical disk drive," *Microsyst. Technol.*, vol. 11, no. 8–10, pp. 1085–1093, Aug. 2005.

[12] T. Atsumi, A. Okuyama, and S. Nakagawa, "Vibration control above the Nyquist frequency in hard disk drives," *IEEE Trans. Ind. Electron.*, vol. 55, no. 10, pp. 3751–3757, Oct. 2008.

[13] K. Thongpull, N. Jindapetch, and W. Teerapabkajorndet, "Wireless ESD event locator systems in hard disk drive manufacturing environments," *IEEE Trans. Ind. Electron.*, vol. 60, no. 11, pp. 5252–5259, Nov. 2013.

[14] T. Atsumi and W. C. Messner, "Optimization of head-positioning control in a hard disk drive using the RBode plot," *IEEE Trans. Ind. Electron.*, vol. 59, no. 1, pp. 521–529, Jan. 2012.

[15] K.-H. Kim, S.-Y. Lee, and S. Kim, "A mobile auto-focus actuator based on a rotary VCM with the zero holding current," *Opt. Exp.*, vol. 17, no. 7, pp. 5891–5896, Mar. 2009.

[16] C.-S. Liu and P. D. Lin, "A miniaturized low-power VCM actuator for auto-focusing applications," *Opt. Exp.*, vol. 16, no. 4, pp. 2533–2540, Feb. 2008.

[17] Y. Liang *et al.*, "Armature reaction field and inductance of coreless moving-coil tubular linear machine," *IEEE Trans. Ind. Electron.*, vol. 61, no. 12, pp. 6956–6965, Dec. 2014.

[18] P. E. Kakosimos, A. G. Sarigiannidis, M. E. Beniakar, A. G. Kladas, and C. Gerada, "Induction motors versus permanent-magnet actuators for aerospace applications," *IEEE Trans. Ind. Electron.*, vol. 61, no. 8, pp. 4315–4325, Aug. 2014.

[19] D.-J. Lee, K.-S. Woo, N.-C. Park, and Y.-P. Park, "Design and optimization of a linear actuator for subminiature optical storage devices," *IEEE Trans. Magn.*, vol. 41, no. 2, pp. 1055–1057, Feb. 2005.

[20] A. Tenconi, S. Vaschetto, and A. Vigliani, "Electrical machines for high-speed applications: Design considerations and tradeoffs," *IEEE Trans. Ind. Electron.*, vol. 61, no. 6, pp. 3022–3029, Jun. 2014.

[21] M. Cheng, W. Hua, J. Zhang, and W. Zhao, "Overview of stator-permanent magnet brushless machines," *IEEE Trans. Ind. Electron.*, vol. 58, no. 11, pp. 5087–5101, Nov. 2011.

[22] I. Petrov and J. Pyrhonen, "Performance of low-cost permanent magnet material in PM synchronous machines," *IEEE Trans. Ind. Electron.*, vol. 60, no. 6, pp. 2131–2138, Jun. 2013.

[23] W. Zhao, T. A. Lipo, and B.-I. Kwon, "Material-efficient permanent-magnet shape for torque pulsation minimization in SPM motors for automotive applications," *IEEE Trans. Ind. Electron.*, vol. 61, no. 10, pp. 5779–5787, Oct. 2014.

[24] D.-J. Lee *et al.*, "Development of 'L-Shaped' rotary voice coil motor actuator for ultra slim optical disk drive using integrated design method based on coupled-field analysis," *Jpn. J. Appl. Phys.*, vol. 46, no. 6S, pp. 3715–3723, Jun. 2007.

[25] H. Lin, Q. Li, Z. He, and S. Chen, "Development of a single coil coupled force VCM actuator for high TPI magnetic recording," *IEEE Trans. Magn.*, vol. 37, no. 2, pp. 850–854, Mar. 2001.

[26] K. Halbach, "Design of permanent multi pole magnets with oriented area earth cobalt material," *Nucl. Instrum. Methods*, vol. 169, no. 1, pp. 1–10, Feb. 1980.

[27] S. Dwari and L. Parsa, "Design of Halbach-array-based permanent-magnet motors with high acceleration," *IEEE Trans. Ind. Electron.*, vol. 58, no. 9, pp. 3768–3775, Sep. 2011.

[28] Q.-S. Lee, K. H. Park, M.-C. Paek, and K.-Y. Kang, "Halbach-magnet-array-based focusing actuator for small-form-factor optical storage device," *Jpn. J. Appl. Phys.*, vol. 45, no. 2S, pp. 1131–1136, Feb. 2006.

[29] Y. Choi, D. Ahn, D. Gweon, and J. Jeong, "Halbach magnetic circuit for voice coil motor in hard disk drives," *J. Magn.*, vol. 15, no. 3, pp. 143–147, Sep. 2010.

[30] K. I. Laskaris and A. G. Kladas, "Permanent-magnet shape optimization effects on synchronous motor performance," *IEEE Trans. Ind. Electron.*, vol. 58, no. 9, pp. 3776–3783, Sep. 2011.

[31] K. I. Laskaris and A. G. Kladas, "Internal permanent magnet motor design for electric vehicle drive," *IEEE Trans. Ind. Electron.*, vol. 57, no. 1, pp. 138–145, Jan. 2010.

Kristopher J. Smith received the B.Sc.(Hons.) degree in communications and electronic engineering and the M.Sc. degree in microelectronic engineering from Northumbria University, Newcastle upon Tyne, U.K., and the Eng.D. degree in engineering from Newcastle University, Newcastle upon Tyne, with a sponsorship from Dyson. His Eng.D. research focused on power supply quality in brushless drives.

Prior to attending Northumbria University, he completed an apprenticeship with British Telecom. After completing the Doctorate degree, he moved into a Teaching Fellowship at Newcastle University. His research interests are mainly in permanent-magnet machine design.

David J. Graham received the B.Eng. degree in electronic engineering and the Ph.D. degree in electronic communications from Newcastle University, Newcastle upon Tyne, U.K., in 2007 and 2011, respectively. His Ph.D. study focused on through-metal communications and power delivery.

Since graduating, he has worked as a Research Associate in the Communications, Sensors, Signal and Information Processing Research Group (ComS2IP) with Newcastle University. His research interests include acoustic communication, digital signal processing, wireless sensor networks, and medical imaging.

Jeffrey A. Neasham received the B.S. degree in electronic engineering from Newcastle University, Newcastle upon Tyne, U.K., in 1994.

He then worked at Newcastle University until 2007 as a Research Associate on research and commercial product development in underwater acoustic communication, sonar imaging, and wireless sensor networks, before taking up an academic post. He is currently a Senior Lecturer of communications and signal processing with the School of Electrical and Electronic Engineering, Newcastle University.